**Title page**

**Title**

The $m^6A$ reader IGF2BP3 promotes gastric cancer progression via increasing the expression of FBXO32 protein

**Authors' names**

Yi Si[1#], Bo Tian[1#], Rui Zhang[1], Mingda Xuan[1], Kunyi Liu[1], Jiao Jiao[1], Shuangshuang Han[1], Hongfei Li[1], Yanhong Hu[1], Hongyan Zhao[1], Wenjing He[2], Jia Wang[3*], Ting Liu[1*], Weifang Yu[1*]

[1] Department of Endoscopy Center, The First Hospital of Hebei Medical University, Shijiazhuang, China

[2] Department of Endoscopy Center, Kuancheng manchu autonomous county hospital, Chengde, China

[3] Department of Infectious Diseases, The First Hospital of Hebei Medical University, Shijiazhuang, China

# These authors contributed equally

*The corresponding authors.

**Corresponding author:** Weifang Yu, M.D., Professor, No. 89 Donggang Road, Shijiazhuang, Hebei, China. E-mail: yuweifang@hebmu.edu.cn. Ting Liu, No. 89 Donggang Road, Shijiazhuang, Hebei, China. E-mail: 59103696@hebmu.edu.cn. Jia Wang, Professor, No. 89 Donggang Road, Shijiazhuang, Hebei, China. E-mail: 57101040@hebmu.edu.cn

22 **Running title**

23 IGF2BP3 promotes GC by regulating FBXO32

24 **Keywords:** IGF2BP3; N6-methyladenosine ($m^6A$); FBXO32; Gastric cancer; Cell

25 biology

26

**Abstract**

N6-methyladenosine ($m^6A$) is the most common chemical modification of eukaryotic mRNAs, and there is increasing evidence that it plays a vital role in human cancer. However, the relationship between the $m^6A$ reader, IGF2BP3, and gastric cancer (GC) has not been fully elucidated. Compared with adjacent normal tissues, the expression level of IGF2BP3 in GC tissues was significantly elevated, which was associated with lymph node metastasis and advanced TNM stage. After the expression level of IGF2BP3 was knocked down in GC cells, the proliferation, migration and invasion ability of the cells were significantly inhibited, the apoptosis level increased, and the levels of glucose, lactic acid and ATP in the cells significantly decreased. When IGF2BP3 was overexpressed, the cell showed the opposite effect. Knocking down IGF2BP3 can inhibit the growth of GC xenografts *in vivo*. Through RNA-seq, MeRIP-seq, RIP-seq and bioinformatics analysis, it was determined that the downstream target gene of IGF2BP3 in GC was FBXO32, which was highly expressed in GC. The interaction between IGF2BP3 and FBXO32 was confirmed by RIP-qPCR, Co-IP and Co-IF. Subsequently, qRT-PCR, WB and rescue studies confirmed that IGF2BP3 could regulate the expression of FBXO32 protein, and the effect of IGF2BP3 on GC cell function was influenced by FBXO32. In summary, our research reveals that IGF2BP3 regulates the expression of FBXO32 protein in an $m^6A$-dependent manner, thereby promoting the progression of GC. The IGF2BP3-FBXO32 axis is crucial for GC occurrence and development and is expected to serve as a potential novel target for the development of GC therapeutics.

## Introduction

Gastric cancer (GC) is a heterogeneous disease characterized by significant differences in epidemiology and histopathology across countries and is one of the leading causes of cancer-related deaths[1]. The morbidity and mortality rates of GC are high worldwide and particularly in China, posing a serious threat to human health[2]. Typically, there are no obvious clinical symptoms in the early stage of GC, and most patients are diagnosed at an advanced stage. The recurrence rate of advanced GC is high, leading to a poor overall prognosis for GC patients[3]. To date, the specific molecular mechanisms of GC have not been fully elucidated. This may be attributed to its complex etiology, which primarily involves the interactions between oncogenes and tumor suppressor genes[4], as well as genetic, epigenetic, and environmental factors[5]. Therefore, further exploration of the molecular mechanisms underlying the occurrence and development of GC will provide potential new targets for the clinical treatment of GC, which is of significant clinical importance.

In recent years, the role of epigenetics in the pathogenesis of GC has attracted extensive attention from scholars worldwide. Epigenetics is generally defined as the study of chemical modifications to DNA and RNA, which mainly include DNA and RNA methylation, histone modification, non-coding RNA modification, and chromatin rearrangement[6]. N6-methyladenosine ($m^6A$) modification is an integral part of epigenetics research. $m^6A$ modification is the most common internal modification of eukaryotic mRNA, regulating the stability, translation efficiency, alternative splicing

and localization of RNA at the post-transcriptional level. It participates in various biological processes such as initiation, proliferation, differentiation, metastasis and metabolic reprogramming of tumor cells[7, 8]. $m^6A$ related proteins are mainly divided into methyltransferase, demethylase and reader proteins, involving 21 related genes[9]. By analyzing the expression of $m^6A$ related proteins in GC and adjacent normal tissues in the TCGA and GEO (GSE54129 and GSE66229 data sets) databases, we screened out four 'readers', YTHDF1, YTHDF2, IGF2BP1 and IGF2BP3, whose expression levels were higher in cancer tissues than in adjacent normal tissues in the above databases. Among these, the expression difference of IGF2BP3 was the most significant, and there are few studies about IGF2BP3 and GC, so IGF2BP3 was selected as the research target. It is reported that the main function of $m^6A$ 'readers' is to interpret RNA methylation modification information and regulate the translation and degradation of its downstream RNA[10, 11].

Insulin like growth factor II mRNA binding protein 3 (IGF2BP3), an $m^6A$ 'reader', is located on human chromosome 7p15.3 and contains two RNA recognition motifs and four K homologous domains[12]. Overexpression of IGF2BP3 was first observed in pancreatic cancer[13]. Its primary role is to recognize $m^6A$ binding sites through the K homology domain, thereby increasing the stability and translation efficiency of target mRNAs[14]. IGF2BP3 is implicated in the development of various cancers, playing distinct roles in each, such as, IGF2BP3 enhances the stability of TMBIM6 mRNA by identifying the $m^6A$ site, thus promoting the progression of laryngeal squamous cell carcinoma[15]; Similarly, IGF2BP3 stabilizes lnc-CTHCC by recognizing its $m^6A$ site,

which increases lnc-CTHCC expression in hepatocellular carcinoma, ultimately facilitating the disease's progression[16]; In colorectal cancer, IGF2BP3 stabilizes CCND1 mRNA by identifying its $m^6A$ site, promoting CCND1 protein expression, regulating the cell cycle, and thus promoting the proliferation and growth of cancer cells[17]; Furthermore, Wang et al. found that $m^6A$ 'reader' IGF2BP2 enhances the stability of GLUT1 mRNA, a key gene in aerobic glycolysis, in an $m^6A$ dependent manner, significantly promoting the aerobic glycolysis of colorectal cancer cells[18]. Therefore, IGF2BP3 may be a critical oncogene. We observed that IGF2BP3 was highly expressed in GC and was closely related to lymph node metastasis and poor prognosis in GC patients. IGF2BP3 reinforces the malignant phenotype of GC cells and inhibit the growth of GC *in vivo*. Through omics analysis, we identified for the first time that the downstream gene with $m^6A$ modification of IGF2BP3 in GC is FBXO32, which is also highly expressed in GC and interacts with IGF2BP3. IGF2BP3 increases FBXO32 protein expression in an $m^6A$ dependent manner and ultimately promotes GC progression.

## Materials and Methods

### Patients and samples

50 pairs of GC tissues and adjacent normal tissues were obtained from the First Hospital of Hebei Medical University. None of the patients had received radiation or chemotherapy prior to surgery and they had signed informed consent forms. The above tissue samples were promptly placed in liquid nitrogen after isolation, and then

115 transferred to the Biological Sample Bank of the First Hospital of Hebei Medical
116 University for storage. The cancer tissues used in this study were pathologically
117 confirmed as gastric adenocarcinoma/signet-ring cell carcinoma. This study was
118 approved by the Ethics Committee of the First Hospital of Hebei Medical University
119 (Approval letter No. S00180) and adheres to the principles of the Declaration of
120 Helsinki.

121 **Cell culture**

122 Human gastric mucosa cell (GES-1) and GC cells (HGC-27, MKN7, MKN74) were
123 obtained from Wuhan Pricella Biotechnology Co., Ltd., and were verified by STR
124 analysis. The cells were cultured in RPMI 1640 medium (Gibco, Gaithersburg, MD,
125 USA) supplemented with 10% fetal bovine serum (FBS; Gibco) and 1% penicillin-
126 streptomycin solution (Solarbio Sciences & Technology Co. Ltd, Beijing, China). They
127 were maintained in a constant temperature and humidity incubator with 5% carbon
128 dioxide at 37°C, and routine mycoplasma detection was performed monthly using PCR.
129 In all experiments, the cells were used for a maximum of no more than 25 passages.

130 **Plasmids, siRNAs, shRNAs, Transfections and Stable cell lines**

131 Transfection was performed according to Lipofectamine 3000 (Invitrogen, Carlsbad,
132 CA, USA) when the cell confluence reached 80-90% in a cell culture flask or dish.
133 IGF2BP3 siRNA and negative control (GenePharma Co., Ltd., Shanghai, China) were
134 transfected into HGC-27 and MKN74 cells, while an IGF2BP3 overexpression plasmid
135 and a negative control (GenePharma) were transfected into MKN7 and GES-1 cells.
136 Additionally, IGF2BP3 shRNA and a negative control (GenePharma) were transfected

137 into HGC-27 cells. FBXO32 siRNA and a negative control (GenePharma) were
138 transfected into MKN7 cells, and an FBXO32 overexpression plasmid and a negative
139 control (GenePharma) were transfected into HGC-27 cells. Follow-up experiments
140 were conducted 48 hours after transfection. To eatablish stable transfected cell lines
141 (HGC-27 shNC, HGC-27 shIGF2BP3), the cell culture medium was changed to include
142 neomycin at a final concentration of 600 μg/mL (without other antibiotics) 48 hours
143 after transfection with IGF2BP3 shRNA in HGC-27 cells. Once the clones have formed,
144 the neomycin concentration was adjusted to 300 μg/mL, continue culturing until day
145 10.

146 **RNA extraction and qRT-PCR**

147 Total RNA was extracted from cells and tissues using RNA-Easy Isolation Reagent
148 (Vazyme Biotech Co.,Ltd., Nanjing, China). The RNA was then reverse-transcribed
149 into complementary DNA (cDNA) following the instructions of PrimeScript RT reagent
150 kit (Takara, Beijing, China). qRT-PCR was performed using the AceQ Universal SYBR
151 qPCR Master Mix (Vazyme), with β-actin serving as the endogenous control mRNA.
152 Each sample was tested in triplicate. The mRNA expression level was determined based
153 on the CT (cyclic threshold) value of each sample, and the relative expression level of
154 each sample was calculated using the 2^-ΔΔCT method. The sequence of primers are
155 detailed in Supplementary Table 1.

156 **Immunohistochemistry (IHC)**

157 Tissues from patients and nude mice were fixed with 4% paraformaldehyde, followed
158 by paraffin embedding (Shanghai YiYang Instrument Co., Ltd., Shanghai, China),

159 sectioning, and staining. The Rabbit/Mouse two-step detection kit (Beijing ZSBG-Bio
160 Co., Ltd., Beijing, China) was used for immunohistochemical analysis according to the
161 manufacturer's instructions. Anti-IGF2BP3 (diluted 1:100; Proteintech, Wuhan, Hubei,
162 P.R.C; Catalog number: 14642-1-AP), Anti-Ki67(diluted 1:100; Proteintech; Catalog
163 number: 27309-1-AP) and Anti-FBXO32(diluted 1:100; Proteintech; Catalog number:
164 67172-1-Ig) antibodies were used for immunohistochemical staining. The staining
165 results were analyzed by using a double-blind scoring method and the average optical
166 density (AOD) method.

167 **Western blot analysis and antibodys**

168 Protein was extracted using RIPA lysis buffer (Solarbio) and the protease inhibitor
169 PMSF (Solarbio) at a ratio of 100:1. The proteins were separated electrophoretically on
170 a 10% SDS polyacrylamide gel (Bio-Rad Laboratories Inc, Hercules, CA, USA) and
171 transferred to a polyvinylidene fluoride membrane (Merck Millipore, Billerica, MA,
172 USA). The following antibodies were used in this study: IGF2BP3 antibody (diluted
173 1:1000; Abcam, Cambridge, MA, USA; Catalog number: ab177477), β-actin antibody
174 (diluted 1:1500; ZSBG-Bio; Catalog number: TA-09), FBXO32 antibody (diluted
175 1:500; Abcam; Catalog number: ab168372) and GAPDH antibody (diluted 1:500;
176 Goodhere Co. Ltd, Hangzhou, China; Catalog number: AB-P-R 001). The
177 immunoreactive protein bands were detected by the Odyssey Scanning System (LI-
178 COR Biosciences, Lincoln, NE, USA).

179 **Cell proliferation assay**

180 For CCK-8 assay, the cells of each group were uniformly distributed in 96-well plates

181 with a density of $1\times10^3$ cells per well, and cultured with complete culture medium. At
182 24, 48, 72, and 96 hours after distribution, 10 μL of Cell Counting Kit -8 (CCK-8;
183 Dojindo, Tokyo, Japan) reagent was added to each well. Then, the cells were incubated
184 in the incubator for an additional 2 hours. The absorbance of each well at 450 nm was
185 measured using a Promega GloMax luminescence detector (Promega, Madison, WI,
186 USA).
187 For the colony formation assay, cells of each group were uniformly distributed in 6-
188 well plates at a density of 500 cells per well. Fresh culture medium was replaced every
189 3 days. Cells were cultured for 7-14 days, then washed twice with PBS, treated with 4%
190 paraformaldehyde for 30 minutes, and stained with 0.1% crystal violet for 20 minutes.
191 **Cell migration assay**
192 For the wound healing assay, the cells of each group were uniformly distributed in 6-
193 well plates. When the cell confluence reached or was close to 100%, a 200 μL pipette
194 tip was used to draw two straight lines on each well to simulate the wound. The cells
195 were then washed twice with PBS and cultured with a culture medium without FBS.
196 Each well was photographed at 0 hours and 48 hours after the wound was created, and
197 the migration rate was expressed as the ratio of gap width measured at 48 hours to the
198 gap width measured at 0 hour.
199 For the Transwell migration assay, $3\times10^4$ (HGC-27, GES-1) /$1\times10^5$ (MKN7, MKN74)
200 cells were added to the upper chamber (Corning Incorporated, Corning, NY, USA) in
201 200 μL FBS-free medium. To induce downward migration, 700 μL of complete medium
202 was added to the lower chamber. After 48 hours of culture, cells on the upper chamber

203 side of the polycarbonate membrane were removed using a swab. The chamber was
204 cleaned twice with PBS, then treated with 4% paraformaldehyde for 30 minutes,
205 followed by 0.1% crystal violet for 20 minutes. The excess crystal violet was cleaned
206 again with PBS. Five visual fields were randomly selected for photography, and the
207 stained cells were counted using ImageJ software (National Institutes of Health,
208 Bethesda, MD, USA).

209 **Cell invasion assay**

210 For the Transwell invasion assay, cells were resuspended in 100 μL FBS-free medium
211 and added to the upper chamber, while 500 μL of complete medium was added to the
212 lower chamber to induce downward invasion of the cells in the upper chamber. All other
213 experimental procedures were the same as those for the Transwell migration assay.

214 **Cell apoptosis assay**

215 Cells from each group were collected 48 hours after transfection and stained using the
216 Annexin V-FITC/PI apoptosis assay kit (NeoBioscience, Shenzhen, China). Flow
217 cytometry (BD Biosciences, San Jose, CA, USA) was used to analyze the apoptosis of
218 $1\times10^5$ cells, and FlowJo software was used to calculate the percentage of apoptotic
219 cells.

220 **Cell glucose metabolism assay**

221 MKN7/HGC-27 cells that overexpressed or have knockdown of IGF2BP3 were
222 collected and processed according to the kit instructions (Glucose Assay kit, Abcam,
223 ab65333; L- Lactate Assay kit, Abcam, ab65331; ATP Assay Kit, Abcam, ab83355). In
224 brief, the standard solutions of glucose, lactic acid and ATP were prepared in a gradient

225 dilution. The reaction mixtures were then prepared, and the diluted standard solutions
226 were mixed with the reaction mixtures for incubation (37℃ or room temperature) for
227 30 minutes. The spectrophotometer was adjusted to the corresponding wavelength to
228 read the absorbance value, and the standard curve for glucose, lactic acid and ATP were
229 generated. The corresponding reagents from the kits were added to the lysed cells, and
230 the cell lysate was deproteinized using Deproteinizing Sample Preparation Kit - TCA
231 (Abcam; Catalog number: ab204708). The deproteinized cell lysates were then mixed
232 with the reaction mixtures for incubation (37℃ or room temperature) for 30 minutes,
233 and the absorbance values were compated to the standard curves to calculate the
234 concentrations of glucose, lactic acid and ATP.

235 **Animal studies**

236 Ten male BALB/c nude mice aged 4-6 weeks, 16-20 g (procured from Beijing
237 Huafukang Biotechnology Co., LTD.) were randomly divided into two groups (five
238 mice per group) and housed in a pathogen-free environment with sufficient water and
239 food. The room temperature was maintained at approximately 22℃ and a 12/12-hour
240 light/dark cycle. In a clean bench, the skin of the left hind limb flank of the nude mice
241 was disinfected, and HGC-27 cells ($5\times10^6$ cells per mice) stably transfected with
242 shRNA-NC and shRNA-IGF2BP3 were subcutaneously injected using a sterile syringe.
243 Starting from day 3 post-injection, tumor size was evaluated every two days using the
244 formula: volume = (long diameter × short diameter $^2$)/2. When the tumor volume
245 approached 1000 $mm^3$, the nude mice were euthanized humanely. Tumor specimens
246 were collected, photographed, weighed, and fixed in formalin. The tumor samples were

247 then paraffin-embedded and sectioned for subsequent HE and IHC analysis. The above
248 experiments were approved by the Ethics Committee of the First Hospital of Hebei
249 Medical University and carried out in accordance with the experimental animal care
250 and use system.

251 **RNA sequencing (RNA-seq)**

252 Total RNA was extracted from HGC-27 cells transfected with siRNA-NC and siRNA-
253 IGF2BP3 for 24 hours. The RNA library construction and sequencing analysis were
254 entrusted to Beijing Novogene Technology Co., LTD. In short, a total of six samples
255 (siNC × 3, siIGF2BP3 × 3) were tested using Illumina's NovaSeq 6000 platform.
256 Quality control and filtering are carried out on the output data from each sample to
257 obtain high-quality data. HISAT software was used to align high-quality data to
258 reference genomes and to quantify gene or transcript expression levels in the sample.
259 DESeq2 software was used for differential expression analysis, with differential genes
260 defined as those with $\log_2|\text{Fold Change}| > 1.0$ and $P < 0.05$ were selected.

261 **Methylated RNA immunoprecipitation sequencing (MeRIP-seq)**

262 Total RNA was extracted from HGC-27 cells transfected with siRNA-NC and siRNA-
263 IGF2BP3 for 24 hours. The RNA library construction and sequencing analysis were
264 entrusted to Novogene. In short, the original data was processed using fastp (version
265 0.19.11) to obtain high quality data. The reference genome index was constructed using
266 BWA (version 0.7.12), and the high-quality data was aligned with the reference genome
267 using BWA mem (version 0.7.12). After mapping reads to the reference genome, the
268 $m^6A$ peaks within each group were identified using the exomePeak R package (version

269 2.16.0). The genes corresponding to each peak were presumed to be peak-related genes.
270 The $m^6A$ enrichment motif of each group was identified by HOMER (version 4.9.1).
271 The peak distribution in the 5' UTR, CDS, 3' UTR and other functional regions on
272 mRNA transcripts was statistically analyzed.

273 **RNA immunoprecipitation and high-throughput sequencing assay (RIP-seq)**

274 According to the instructions of the RNA Immunoprecipitation (RIP) Kit（BersinBio,
275 Guangzhou, China; Catalog number: Bes5101）, HGC-27 cells transfected with siRNA-
276 NC and siRNA-IGF2BP3 for 48 hours were collected and lysed. An IGF2BP3 specific
277 antibody (10 μg; Proteintech; Catalog number: 14642-1-AP) was employed to bind the
278 endogenous expression of IGF2BP3 protein in the cells, precipitate the target protein-
279 RNA complex, and subsequently isolate and purify the RNA within the complex.
280 Novogene was commissioned to perform ribosomal RNA removal, RNA library
281 construction and high-throughput sequencing analysis. In brief, RNA fragment
282 distribution and concentration after immunoprecipitation and ribosomal RNA removal
283 were measured using an Agilent 2100 bioanalyzer (Agilent) and a simpliNano
284 spectrophotometer (GE Healthcare). The library was constructed using the NEB
285 Next®Ultra™RNA Library Preparation Kit (New England Biolabs). The library quality
286 was assessed using the Agilent Bioanalyzer 2100 system and then sequenced using the
287 Illumina Novaseq platform. The fastp software was utilized to filter the original data
288 and obtain high-quality data. The reference genome index was established using BWA
289 (version 0.7.12), and the filtered data was compared with the reference genome using
290 BWA mem (version 0.7.12). After the comparison was completed, the IP enrichment

291 region was identified against the background using MACS2(version 2.1.0) peak call
292 software. After peak calling was completed, the results were analyzed for chromosome
293 distribution, peak width, fold abundance, significance level and peak number per peak.
294 Homer (version 4.9.1) software was used to identify $m^6A$ enrichment motifs in each
295 group. Peak Annotator software was used to identify peak-related genes. Differential
296 peak analysis was carried out based on the different enrichment times of the peaks in
297 the results, and then the genes related to the difference peak were identified.

298 **Co-Immunofluorescent (Co-IF) assay**

299 HGC-27 cells were evenly distributed on coverslips in a 6-well plate. When the cell
300 fusion rate reached 20-30%, the cells were gently rinsed with PBS for three times.
301 Subsequently, the cells were fixed with 4% paraformaldehyde, permeated with 0.2%
302 Triton X-10 (Solarbio; Catalog number: T8200), and blocked with 2% bovine serum
303 albumin (BSA-V; Solarbio; Catalog number: A8020). The cells were then incubated
304 overnight at 4℃ with IGF2BP3 antibody (diluted 1:50; Proteintech; Catalog number:
305 14642-1-AP) and FBXO32 antibody (diluted 1:50; Proteintech; Catalog number:
306 67172-1-Ig). Following this, the cells were incubated with fluorescent secondary
307 antibody (diluted 1:500; Cy3 anti-rabbit IgG, FITC anti-mouse IgG; Beyotime
308 Biotechnology Co., Shanghai, China) at room temperature for 1 hour in a dark
309 environment. Finally, 4 '6' -diamino-2-phenylindole dihydrochloride (DAPI; Beyotime
310 Biotechnology Co.) was used to stain the nuclei. Representative images were captured
311 using a laser scanning confocal microscope (ZEISS, Oberkochen, Germany).

312 **Co-immunoprecipitation (Co-IP)**

313 HGC-27 cells were harvested and gently washed twice with PBS. Subsequently, cell
314 lysis was performed following the protocol outlined in the Pierce™ Classic Magnetic
315 IP/Co-IP Kit (Thermo Scientific, Waltham, USA; Catalog number: 88804). Following
316 lysis, IGF2BP3 antibody (10 μg; Proteintech), FBXO32 antibody (10μg; Proteintech)
317 and IgG antibody (10 μg; Proteintech) were individually added to the cell lysate and
318 allowed to incubate for 2 hours at room temperature. Magnetic beads were added into
319 the lysate and the mixture was continuously rotated at room temperature for 1 hour. The
320 magnetic beads were then isolated using a magnetic rack and the protein was eluted by
321 utilizing Elution Buffer. Neutralization Buffer was added to adjust the pH to neutral.
322 The resultant samples were subsequently utilized for Western blot analysis.

323 **Bioinformatics analysis**

324 The expression of IGF2BP3 mRNA in cancer and adjacent tissues of patients with GC
325 was obtained from TCGA (https://www.aclbi.com/static/index.html#/tcga) and GEO
326 (https://www.aclbi.com/static/index.html#/geo) databases. The online website Kaplan-
327 Meier Plotter (https://kmplot.com/analysis/) was used to analyze the influence of gene
328 expression level on the prognosis of GC patients. GEPIA2 (http://gepia2.cancer-
329 pku.cn/#index) was used to analyze gene expression levels in GC and adjacent normal
330 tissues, while GeneCards (https://www.genecards.org/) provided insight into gene
331 sublocalization within cells. PrimerBank (https://pga.mgh.harvard.edu/primerbank/)
332 and the Primer designing tool (https://www.ncbi.nlm.nih.gov/tools/primer-blast/) were
333 employed for primer prediction. BioRender (https://www.biorender.com/) facilitated
334 the creation of scientific schematic diagrams, and catRAPID omics

335 (http://s.tartaglialab.com/page/catrapid_group) was used to predict binding site motifs
336 between the IGF2BP3 protein and FBXO32 mRNA. The iGV software was utilized for
337 the analysis of genomic $m^6A$ methylation levels.

338 **Statistical analysis**

339 In this study, three independent replicates were performed for each group of
340 experiments. The results of normal distribution data were presented as mean ± standard
341 deviation, while non-normally distributed data were presented as median and
342 interquartile distance. Statistical analysis in this study was processed using GraphPad
343 Prism 9.5 (GraphPad Software, La Jolla, CA, USA) and SPSS 26.0 (IBM, Armonk, NY,
344 USA). Statistical methods including Student's *t*-test, one-way ANOVA and two-way
345 ANOVA were employed. A significance level of $P<0.05$ was considered statistically
346 significant.

347

348 **Results**

349 **IGF2BP3 is upregulated in GC patients and is associated with poor prognosis**

350 To investigate the role of $m^6A$ related genes in the pathogenesis of GC, we first analyzed
351 the expression of 21 $m^6A$ related genes in GC and adjacent normal tissues in the TCGA
352 database and the GSE54129 and GSE66229 datasets (Figure 1A-C). Four $m^6A$ reader
353 proteins (YTHDF1, YTHDF3, IGF2BP1 and IGF2BP3) with higher expression levels
354 in GC than in adjacent normal tissues were screened. Among them, IGF2BP3 exhibited
355 the most significant differential expression, and due to the limited research on its
356 mechanism in GC, we selected IGF2BP3 as our research focus. Kaplan-Meier survival

357 analysis suggested that GC patients with high IGF2BP3 expression had worse overall
358 survival compared to those with low IGF2BP3 expression (Figure 1D). We then
359 assessed IGF2BP3 mRNA expression in 50 pairs of fresh frozen GC tissues and
360 adjacent normal tissues using qRT-PCR. Consistent with the TCGA and GEO data, the
361 expression of IGF2BP3 was significantly higher in GC tissues compared to adjacent
362 normal tissues, with a statistically significant difference ($P<0.01$) (Figure 1E). IHC
363 was employed to detect IGF2BP3 protein expression in these samples. The results
364 showed that IGF2BP3 protein was primarily localized in the cytoplasm of GC cells,
365 and was expressed at significantly higher levels than in adjacent normal tissues
366 ($\chi^2=18.382$), with a statistically significant difference ($P<0.001$) (Figure 1F, Table 1).
367 Finally, we analyzed the protein expression of IGF2BP3 in GC tissues alongside clinical
368 data from the corresponding patients. We found that patients with lymph node
369 metastasis or advanced TNM stage had higher levels of IGF2BP3 expression (both $P$
370 $<0.01$) (Table 2). These findings suggest that the $m^6A$ reader protein IGF2BP3 is
371 highly expressed in GC and is closely associated with poor prognosis in GC patients.

372 **IGF2BP3 knockdown suppress the progression of GC *in vitro***

373 In order to explore the mechanism of IGF2BP3 in GC, we first downregulated IGF2BP3
374 expression in HGC-27 and MKN74 cell lines and observed the effects on various
375 cellular functions. Following transfection with siRNA targeting IGF2BP3 (siIGF2BP3)
376 and a siRNA negative control (siNC), both the mRNA (Figure 2A, B) and protein
377 (Figure 2C, D) levels of IGF2BP3 were significantly reduced. The CCK-8 assay
378 revealed that cells proliferation was markedly inhibited after knockdown of IGF2BP3

379 (Figure 2E, F). The wound healing assay (Figure 2G, H) and Transwell migration assay
380 (Figure 2I, J) demonstrated that the downregulation of IGF2BP3 significantly
381 suppressed cells migration. Furthermore, the Transwell invasion assay indicated that
382 reducing IGF2BP3 expression significantly impaired the invasion capability of the cells
383 (Figure 2K, L). Flow cytometry analysis showed that silencing IGF2BP3 expression
384 promoted the apoptosis of HGC-27 and MKN74 cells (Figure 2M, N). These results
385 suggest that downregulation of IGF2BP3 inhibits proliferation, migration and invasion
386 of GC cells and promotes apoptosis.

387 **Overexpression of IGF2BP3 can promote the progression of GC *in vitro***

388 We upregulated the expression of IGF2BP3 in MKN7 and GES-1 cell lines to observe
389 its effect on cellular biological functions. After transfecting the cells with pcDNA3.1-
390 IGF2BP3 (IGF2BP3) and pcDNA3.1-vector (Vector), we obversed a significant
391 increase in IGF2BP3 mRNA (Figure 3A, B) and protein (Figure 3C, D) levels. The
392 CCK-8 assay demonstrated a notable enhancement in cell proliferation following after
393 the overexpression of IGF2BP3 (Figure 3E, F). Both the wound healing assay (Figure
394 3G, H) and the Transwell migration assay (Figure 3I, J) indicated that upregulating
395 IGF2BP3 significantly strengthened the cells' migration capability. Furthermore, the
396 Transwell invasion assay revealed that elevated IGF2BP3 expression significantly
397 heightened the invasion ability of cells (Figure 3K). The flow cytometry analysis
398 revealed that increased IGF2BP3 expression led to a reduction in apoptosis levels in
399 both MKN7 and GES-1 cell lines (Figure 3L, M). Despite multiple experiments, GES-
400 1 cells did not demonstrate the ability to penetrate the matrix glue at the base of the

401 Transwell chambers, due to the inherently weaker invasion ability of normal epithelial
402 cells. In summary, these results show that overexpression of IGF2BP3 can promote the
403 proliferation, migration and invasion of GC cells and inhibit their apoptosis, suggesting
404 that IGF2BP3 may play the role of a pro-oncogene in GC.

405 **IGF2BP3 promotes glucose metabolism in GC cells**

406 Tumor cells rapidly produce a large amounts of energy through a unique aerobic
407 glycolysis pathway to meet their surging metabolic demands, thereby maintaining
408 normal cellular functions. We monitored the levels of glucose, lactic acid and ATP in
409 GC cells after modulating the expression of IGF2BP3 to explore its role in glucose
410 metabolism in these cells. The results showed that after down-regulating or up-
411 regulating the expression level of IGF2BP3 in HGC-27 and MKN7 cells, the
412 intracellular levels of glucose (Figure S1A), lactic acid (Figure S1B) and ATP (Figure
413 S1C) were correspondingly decreased or increased. These findings suggest that
414 IGF2BP3 may play a significant role in regulating glucose metabolism in GC cells. In
415 the near future, we will continue to examine changes in the oxygen consumption rate
416 (OCR) and extracellular acidification rate (ECAR) in GC cells after altering IGF2BP3
417 expression, to further explore the effects of IGF2BP3 on the glycolytic capability of
418 these cells.

419 **IGF2BP3 deficiency inhibits the growth of GC *in vivo***

420 In order to further investigate the mechanism of IGF2BP3 in GC *in vivo*, we established
421 tumor bearing nude mice models with low expression of IGF2BP3 and corresponding
422 negative controls. HGC-27 cell lines stably transfected with shRNA-IGF2BP3 and

423 shRNA-negative control were successfully established (shNC/shIGF2BP3) and
424 subsequently injected subcutaneously into two groups of nude mice, respectively. The
425 tumor-bearing models, along with the curves of tumor volume, tumor photographs and
426 weights were presented in Figure 4A-D. The results demonstrated a significant
427 reduction in the growth rate, volume, and weight of tumors in the shIGF2BP3 group
428 compared to those in the shNC group. HE staining was utilized to evaluate the
429 morphological characteristics of the xenograft tissues, and the results indicated that the
430 cell morphology and structure were similar to those of GC tissues (Figure 4E). Ki67
431 immunohistochemical staining indicated that the proliferation ability of cells in the
432 shIGF2BP3 group was significantly inhibited compared with the shNC group (Figure
433 4F). These findings suggest that IGF2BP3 knockdown can inhibit the growth of GC *in*
434 *vivo*.

435 **FBXO32 is the m$^6$A modification target of IGF2BP3 in GC**

436 In order to further explore the potential mechanism of IGF2BP3 in the pathogenesis of
437 GC, we performed RNA-seq, MeRIP-seq, and RIP-seq in HGC-27 cells of siNC group
438 and siIGF2BP3 group, respectively. The RNA-seq results indicated that the expression
439 levels of a total of 388 genes were significantly changed after IGF2BP3 expression was
440 knocked down, including 181 down-regulated genes and 207 up-regulated genes
441 (Figure 5A, B). MeRIP-seq results showed that 25,331 m$^6$A peaks were identified in
442 the siNC group and 26,188 m$^6$A peaks in the siIGF2BP3 group (Figure 5C). When
443 mapping the m$^6$A methyl group in HGC-27 cells, the m$^6$A consistent sequence motif
444 (GGAC) could be identified, indicating successful enrichment of mRNA with m$^6$A

445 modifications (Figure 5D). In addition, $m^6A$ modification was observed to be mainly
446 enriched in the CDS and 3' UTR of mRNA (Figure 5E). Then, the genes corresponding
447 to the $m^6A$ peaks of the siNC group and siIGF2BP3 group were intersected, resulting
448 in the identification of 10,514 genes (Figure 5F). Analysis of the RIP-seq results
449 showed that $m^6A$ modification was also primarily enriched in the CDS and 3' UTR of
450 mRNA (Figure 5G). Specifically, 1,928 and 810 $m^6A$ peaks were identified in siNC
451 group and siIGF2BP3 group, respectively (Figure 5H). After removing the same genes
452 from the $m^6A$ peaks corresponding genes of both group, 73 unique genes were
453 identified (Figure 5I). Subsequent unified analysis of the genes identified by RNA-seq,
454 MeRIP-seq and RIP-seq showed that 19 genes bound to the IGF2BP3 protein were
455 simultaneously labeled by $m^6A$, and none of them had changes in transcription level
456 after IGF2BP3 knockdown. These genes were identified as IGF2BP3 candidate target
457 genes (Figure 5J). Further analysis of these genes included examing their expression in
458 GC tissues, subcellular localization, survival of GC patients associated with these genes,
459 and the abundance and loci of $m^6A$ on their mRNA. The results suggested that FBXO32
460 was highly expressed in GC tissues according to the TCGA database (Figure 5K),
461 predominantly distributed in the cytoplasm and nucleus (Figure 5L), and the overall
462 survival of patients with high expression of FBXO32 was poor (Figure 5M), and the
463 IGF2BP3 binding site was coincide with the $m^6A$ modification site (Figure 5N).
464 Additionally, RIP-qPCR demonstrated that the IGF2BP3 protein could significantly
465 enrich FBXO32 mRNA (Figure 5O). Moreover, as predicted by the catRAPID website,
466 there is a direct binding site between the IGF2BP3 protein and FBXO32 mRNA, as

467 shown in the motif (Figure 5P). Based on the above analysis results, FBXO32 was
468 identified as the $m^6A$ modification target of IGF2BP3 in GC.

469 **FBXO32 is highly expressed in GC and directly interacts with IGF2BP3**

470 Next, we initially verified the expression of FBXO32 in GC cell lines and GC tissues.
471 The results indicated that the level of FBXO32 mRNA in GC cell lines was higher than
472 that in normal gastric mucosa cells (Figure 6A), and in GC tissues, it was higher in
473 adjacent tissues (34 pairs of GC paired tissues) (Figure 6B). The expression of FBXO32
474 protein was highest in MKN7 cells (Figure 6C), and higher in GC tissues than in
475 adjacent tissues (19 pairs of GC paired tissues) (Figure 6D). These results suggest that
476 FBXO32 acts as an oncogene in GC pathogenesis. Subsequently, the interaction
477 between IGF2BP3 and FBXO32 was verified by Co-IP and Co-IF experiments. The
478 Co-IP results showed that IGF2BP3 and FBXO32 can co-precipitate each other in GC
479 cells (Figure 6E). The Co-IF results showed that IGF2BP3 and FBXO32 were mainly
480 located in the cytoplasm and nucleus of GC cells, and they have co-localization (Figure
481 6F). Finally, to further confirm the regulation of FBXO32 expression by IGF2BP3 in
482 GC cells, we examined the transcriptional and translational changes of FBXO32 after
483 IGF2BP3 knockdown or overexpression. After down-regulating the expression level of
484 IGF2BP3 in HGC-27 cells, the expression level of FBXO32 mRNA did not change
485 significantly (Figure 6G), while the expression level of its protein was down-regulated
486 (Figure 6H). Similarly, when IGF2BP3 expression was upregulated in MKN7 cells, the
487 expression level of FBXO32 mRNA was not significantly changed (Figure 6I), while
488 its protein expression level was upregulated (Figure 6J). This phenomenon indicates

489 that IGF2BP3, as an $m^6A$ reader, only regulates the expression of downstream genes at
490 the translation level, not at the transcriptional level, which is consistent with the existing
491 research conclusions on other $m^6A$ readers. In conclusion, these results indicate that
492 IGF2BP3 and FBXO32 interact with each other in GC, and IGF2BP3 can regulate the
493 expression of FBXO32 protein.

494 **The oncogenic effect of IGF2BP3 is dependent on FBXO32 in GC cells**

495 Four siRNA-FBXO32 sequences were transfected simultaneously into MKN7 cells
496 with the highest FBXO32 expression, and one of the siRNA sequences with the most
497 significant knockdown efficiency (si-FBXO32-910) was screened for subsequent
498 experiments (Figure 7A). Next, we transfected siRNA-negative control/siRNA-
499 IGF2BP3 and pcDNA3.1-vector/pcDNA3.1-FBXO32 into HGC-27 and pcDNA3.1-
500 vector/pcDNA3.1-IGF2BP3 and siRNA-negative control/siRNA-FBXO32 into MKN7
501 cells, respectively or simultaneously. The changes of IGF2BP3 expression in each
502 group were detected by qRT-PCR. The results suggest that the knockdown effect of
503 IGF2BP3 in HGC-27 cells could be attenuated by the overexpression of FBXO32
504 (Figure 7B), and the up-regulation effect of IGF2BP3 in MKN7 cells could also be
505 weakened by the knockdown of FBXO32 (Figure 7C). These findings indicate that
506 FBXO32 can affect the expression of IGF2BP3 in GC cells. Subsequently, we further
507 explored whether the effects of IGF2BP3 on GC cell function would be influenced by
508 FBXO32. The results showed that the attenuation of cell proliferation, migration, and
509 invasion induced by knockdown of IGF2BP3 in HGC-27 cells could be rescued by the
510 up-regulation of FBXO32 expression (Figure 7D-H). The enhancement of cell

511 proliferation, migration, and invasion caused by overexpression of IGF2BP3 in MKN7
512 cells could be attenuated by the down-regulation of FBXO32 expression (Figure 7I-M).
513 These results suggest that FBXO32 is a key downstream target for IGF2BP3 promoting
514 GC progression, and that the oncogenic effects of IGF2BP3 in GC cells are dependent
515 on FBXO32. Therefore, we propose that increased IGF2BP3 can bind to more FBXO32
516 mRNA via recognizing the $m^6A$ sites on them, thereby causing increased expression of
517 FBXO32 protein and ultimately promoting tumorigenesis of GC cells (Figure 7N).
518

519 **Discussion**

520 In this study, we report for the first time that IGF2BP3 binds to FBXO32 mRNA by
521 recognizing the $m^6A$ site, resulting in increased intracellular levels of FBXO32 protein,
522 which ultimately promotes the progression of GC. Currently, no optimal prognostic
523 biomarker for GC has been identified. This study also confirmed that IGF2BP3
524 expression is up-regulated in GC and is associated with lymph node metastasis and
525 altered cellular glucose metabolism, revealing its clinical significance and potential
526 value in GC prognosis.
527 Through literature review and database analysis, we found that the expression of
528 IGF2BP3 was most significantly different in GC tissues compared to adjacent normal
529 tissues. However, the relationship between IGF2BP3 and GC remains to be further
530 explored. Previous studies indicate that the expression level of IGF2BP3 in laryngeal
531 squamous cell carcinoma (LSCC) was higher than that in adjacent normal tissues[15].
532 Additionally, the expression of IGF2BP3 is elevated in gallbladder cancer and is

associated with poor prognosis of patients, which can enhance multiple malignant phenotypes of gallbladder cancer cells, and knockdown of IGF2BP3 can inhibit the tumor growth *in vivo*[19]. The expression level of IGF2BP3 in colon cancer is also significantly higher than that in adjacent normal tissues and is associated with worse overall survival. Altering the expression level of IGF2BP3 can regulate the cell cycle and affect cell proliferation, and knocking it down can inhibit the tumor growth of colon cancer *in vivo*[17]. Consistent with these findings, our study revealed that the expression levels of IGF2BP3 mRNA and protein in GC tissues were higher than those in adjacent normal tissue. The increased expression level of IGF2BP3 was closely related to lymph node metastasis and more advanced TNM stage. In our experiments, knocking down the expression level of IGF2BP3 in GC cells significantly inhibited, cell proliferation, migration and invasion, and increased apoptosis. Conversely, upregulating IGF2BP3 expression in GC cells had the opposite effect. Furthermore, we observed that IGF2BP3 deficiency inhibited the growth of GC *in vivo*. These findings suggest that IGF2BP3 may be an important oncogene in GC. Additionally, Wang J et al. found that IGF2BP2 enhanced the stability of GLUT1 mRNA, a key gene of aerobic glycolysis, in an $m^6A$ dependent manner, significantly promoting the aerobic glycolysis in colorectal cancer cells[18]. Our results also showed that after up-regulating or down-regulating the expression level of IGF2BP3 in GC cells, the contents of glucose, lactic acid and ATP in the cells correspondingly increased/decreased. Thus, the effects of IGF2BP3 on the biological function of GC cells may be closely related to the regulation of glucose metabolism in cells, which warrants further exploration.

555 Through RNA-seq, MeRIP-seq, RIP-seq and bioinformatics analysis, we identified
556 FBXO32 as the target of IGF2BP3 with $m^6A$ modification in GC for the first time. F-
557 Box Protein 32 (FBXO32), originally identified as a muscle-specific gene involved in
558 muscle atrophy, is an E3 ubiquitin ligase located on chromosome 8q24.13[20, 21].
559 Previous studies have reported that FBXO32 is involved in various processes such as
560 epithelial-mesenchymal transformation and tumorigenesis[22]. The overexpression of
561 FBXO32 is conducive to the proliferation and migration of melanoma cells, while its
562 downregulation has the opposite effect[23]. FBXO32 is abnormally upregulated in
563 pancreatic ductal adenocarcinoma, promoting the migration and invasion of pancreatic
564 cancer cells *in vitro*, and promoting tumor growth and metastasis *in vivo*[24]. FBXO32
565 enhances the PI3K/AKT/mTOR pathway by degrading PTEN, thereby promoting the
566 progression of lung adenocarcinoma[25]. In this study, the expression levels of FBXO32
567 mRNA and protein in GC tissues were higher than those in adjacent normal tissues, and
568 the expression levels of FBXO32 mRNA and protein in GC cells were also higher than
569 those in normal gastric mucosa cells. These findings suggest that FBXO32 may be an
570 important oncogene in GC. However, there are some results that contradict our
571 conclusions. For example, the expression of FBXO32 is down-regulated in multiple
572 myeloma[26]. Overexpression of FBXO32 can inhibit tumorigenicity of ovarian cancer
573 cells both *in vivo* and *in vitro*[27]. Therefore, the role of FBXO32 in cancer cannot be
574 generalized, and more extensive and in-depth studies are needed to elucidate its
575 mechanisms. Subsequently, Co-IP and Co-IF experiments confirmed that IGF2BP3 and
576 FBXO32 had a direct interaction relationship in GC cells, and this conclusion has not

been reported in existing studies. In addition, as predicted by bioinformatics analysis, there was a binding site between IGF2BP3 protein and FBXO32 mRNA, which further supports our conclusion about their interaction.

To explore the regulatory mechanism of IGF2BP3 on FBXO32 in GC, we demonstrated that IGF2BP3 regulates FBXO32 expression at the translational level but not at the transcriptional level. Previous studies have reported that IGF2BP3 can enhance the translation of COPS7B mRNA and promote the growth and metastasis of colorectal cancer[28]. IGF2BP3 promotes EGFR mRNA translation in an $m^6A$-dependent manner, contributing to CRC progression and cetuximab resistance[29]. Thus, it is possible that IGF2BP3 binds FBXO32 mRNA in an $m^6A$-dependent manner and promotes its translation, ultimately contributing to GC progression. Finally, we also conducted rescue experiment to further verify whether the effect of IGF2BP3 on GC cell function is mediated by FBXO32. The results indicate that FBXO32 is a key downstream target of IGF2BP3 in GC, and the oncogenic effect of IGF2BP3 in GC cells depends on FBXO32.

Admittedly, our research currently has certain limitations. For example, the human tissue samples used for clinical validation were all from the same hospital, and there was a lack of multi-center clinical data. In addition, our findings about the effect of changes in IGF2BP3 expression level on cellular glucose metabolism in GC cells are worthy of further exploration to elucidate the in-depth mechanism of GC and glucose metabolism.

In conclusion, our study identified FBXO32 as a direct target of IGF2BP3 with $m^6A$

599 modification in GC cells. IGF2BP3 promotes the translation of FBXO32 in an $m^6A$-
600 dependent manner, ultimately contributing to the development of GC. Thus, targeting
601 IGF2BP3 might be a promising strategy for GC therapy.
602
603 **Author Contributions**
604 WFY, JW, TL, YS and BT contributed to conception and design, JW, WFY and TL
605 contributed to administrative support, WJH, HYZ and MDX contributed to Provision
606 of study materials or patients, KYL, JJ, HFL and YHH contributed to collection and
607 assembly of data, SSH, BT and YS contributed to data analysis and interpretation, all
608 authors contributed to manuscript writing and final approval of manuscript.
609
610 **Acknowledgments**
611 This work was supported by Hebei Provincial Government-funded Provincial Medical
612 Excellent Talent Project (ZF2023025, ZF2024134, and LS202008), Hebei Natural
613 Science Foundation (H2022206292, H2024206140), Key R&D Program of Hebei
614 Province (223777103D and 223777113D), Prevention and treatment of geriatric
615 diseases by Hebei Provincial Department of Finance (LNB202202, LNB201809 and
616 LNB201909), Spark Scientific Research Project of the First Hospital of Hebei Medical
617 University (XH202312 and XH201805), Hebei Province Medical Applicable
618 Technology Tracking Project (G2019035) and other projects of Hebei Province (1387
619 and SGH201501).
620

## Conflict Of Interest Statement

The authors have no conflicts of interest to declare.

## Data Availability Statement

The data underlying this article will be shared on reasonable request to the corresponding author.

## References

1. Chia NY, Tan P. Molecular classification of gastric cancer[J]. Annals of oncology : official journal of the European Society for Medical Oncology, 2016, 27(5): 763-769.

2. Sung H, Ferlay J, Siegel RL, Laversanne M, Soerjomataram I, Jemal A, Bray F. Global Cancer Statistics 2020: GLOBOCAN Estimates of Incidence and Mortality Worldwide for 36 Cancers in 185 Countries[J]. CA: a cancer journal for clinicians, 2021, 71(3): 209-249.

3. Song Z, Wu Y, Yang J, Yang D, Fang X. Progress in the treatment of advanced gastric cancer[J]. Tumour biology : the journal of the International Society for Oncodevelopmental Biology and Medicine, 2017, 39(7): 1010428317714626.

4. Fukagawa T, Katai H, Mizusawa J, Nakamura K, Sano T, Terashima M, Ito S, Yoshikawa T, Fukushima N, Kawachi Y, Kinoshita T, Kimura Y, Yabusaki H, Nishida Y, Iwasaki Y, Lee SW, Yasuda T, Sasako M. A prospective multi-institutional validity study to evaluate the accuracy of clinical diagnosis of pathological stage III gastric cancer (JCOG1302A)[J]. Gastric cancer : official journal of the International Gastric

643 Cancer Association and the Japanese Gastric Cancer Association, 2018, 21(1): 68-73.
644 5. Arnold M, Karim-Kos HE, Coebergh JW, Byrnes G, Antilla A, Ferlay J, Renehan
645 AG, Forman D, Soerjomataram I. Recent trends in incidence of five common cancers
646 in 26 European countries since 1988: Analysis of the European Cancer Observatory[J].
647 European journal of cancer (Oxford, England : 1990), 2015, 51(9): 1164-1187.
648 6. Tang SY, Zhou PJ, Meng Y, Zeng FR, Deng GT. Gastric cancer: An epigenetic
649 view[J]. World journal of gastrointestinal oncology, 2022, 14(1): 90-109.
650 7. Han X, Wang L, Han Q. Advances in the role of m(6)A RNA modification in cancer
651 metabolic reprogramming[J]. Cell & bioscience, 2020, 10: 117.
652 8. Xie Q, Wu TP, Gimple RC, Li Z, Prager BC, Wu Q, Yu Y, Wang P, Wang Y, Gorkin
653 DU, Zhang C, Dowiak AV, Lin K, Zeng C, Sui Y, Kim LJY, Miller TE, Jiang L, Lee-
654 Poturalski C, Huang Z, Fang X, Zhai K, Mack SC, Sander M, Bao S, Kerstetter-Fogle
655 AE, Sloan AE, Xiao AZ, Rich JN. N(6)-methyladenine DNA Modification in
656 Glioblastoma[J]. Cell, 2018, 175(5): 1228-1243.e1220.
657 9. Yang Y, Hsu PJ, Chen YS, Yang YG. Dynamic transcriptomic m(6)A decoration:
658 writers, erasers, readers and functions in RNA metabolism[J]. Cell research, 2018,
659 28(6): 616-624.
660 10. Lee M, Kim B, Kim VN. Emerging roles of RNA modification: m(6)A and U-tail[J].
661 Cell, 2014, 158(5): 980-987.
662 11. Jacobs BL, Lee CT, Montie JE. Bladder cancer in 2010: how far have we come?[J].
663 CA: a cancer journal for clinicians, 2010, 60(4): 244-272.
664 12. Bell JL, Wächter K, Mühleck B, Pazaitis N, Köhn M, Lederer M, Hüttelmaier S.

Insulin-like growth factor 2 mRNA-binding proteins (IGF2BPs): post-transcriptional drivers of cancer progression?[J]. Cellular and molecular life sciences : CMLS, 2013, 70(15): 2657-2675.

13. Müeller-Pillasch F, Lacher U, Wallrapp C, Micha A, Zimmerhackl F, Hameister H, Varga G, Friess H, Büchler M, Beger HG, Vila MR, Adler G, Gress TM. Cloning of a gene highly overexpressed in cancer coding for a novel KH-domain containing protein[J]. Oncogene, 1997, 14(22): 2729-2733.

14. Liu X, Chen J, Chen W, Xu Y, Shen Y, Xu X. Targeting IGF2BP3 in Cancer[J]. International journal of molecular sciences, 2023, 24(11).

15. Wang X, Tian L, Li Y, Wang J, Yan B, Yang L, Li Q, Zhao R, Liu M, Wang P, Sun Y. RBM15 facilitates laryngeal squamous cell carcinoma progression by regulating TMBIM6 stability through IGF2BP3 dependent[J]. Journal of experimental & clinical cancer research : CR, 2021, 40(1): 80.

16. Xia A, Yuan W, Wang Q, Xu J, Gu Y, Zhang L, Chen C, Wang Z, Wu D, He Q, Yu W, Wang F, Xue C, Zhang Y, Bao G, Tao X, Liu S, Wang S, Hu Z, Sun B. The cancer-testis lncRNA lnc-CTHCC promotes hepatocellular carcinogenesis by binding hnRNP K and activating YAP1 transcription[J]. Nature cancer, 2022, 3(2): 203-218.

17. Yang Z, Wang T, Wu D, Min Z, Tan J, Yu B. RNA N6-methyladenosine reader IGF2BP3 regulates cell cycle and angiogenesis in colon cancer[J]. Journal of experimental & clinical cancer research : CR, 2020, 39(1): 203.

18. Wang J, Zhu M, Zhu J, Li J, Zhu X, Wang K, Shen K, Yang K, Ni X, Liu X, Zhang G, Xi Q, Shi T, Chen W. HES1 promotes aerobic glycolysis and cancer progression of

687 colorectal cancer via IGF2BP2-mediated GLUT1 m6A modification[J]. Cell death
688 discovery, 2023, 9(1): 411.
689 19. Qin J, Cui Z, Zhou J, Zhang B, Lu R, Ding Y, Hu H, Cai J. IGF2BP3 drives
690 gallbladder cancer progression by m6A-modified CLDN4 and inducing macrophage
691 immunosuppressive polarization. Transl Oncol. 2023 Nov;37:101764.
692 20. Sahu SK, Tiwari N, Pataskar A, Zhuang Y, Borisova M, Diken M, Strand S, Beli P,
693 Tiwari VK. FBXO32 promotes microenvironment underlying epithelial-mesenchymal
694 transition via CtBP1 during tumour metastasis and brain development. Nature
695 communications, 2017, 8(1): 1523.
696 21. Mei Z, Zhang D, Hu B, Wang J, Shen X, Xiao W. FBXO32 Targets c-Myc for
697 Proteasomal Degradation and Inhibits c-Myc Activity. The Journal of biological
698 chemistry, 2015, 290(26): 16202-16214.
699 22. Wang H, Liu H, Zhao L, Luo S, Akinyemiju T, Hwang S, Yue Y, Wei Q. Association
700 of genetic variants of FBXO32 and FOXO6 in the FOXO pathway with breast cancer
701 risk. Molecular carcinogenesis, 2021, 60(10): 661-670.
702 23. Li Y, Gao S, Xue W, Ma Y, Meng Y, Zhang D. miR-19a-3p Functions as an
703 Oncogene by Regulating FBXO32 Expression in Multiple Myeloma. Balkan medical
704 journal, 2021, 38(1): 43-49.
705 24. Su D, Wang R, Chen G, Ding C, Liu Y, Tao J, Wang Y, Qiu J, Luo W, Weng G, Gang
706 Y, Zhang T. FBXO32 Stimulates Protein Synthesis to Drive Pancreatic Cancer
707 Progression and Metastasis. Cancer Res. 2024 May 22.
708 25. Wu J, Wen T, Marzio A, Song D, Chen S, Yang C, Zhao F, Zhang B, Zhao G, Ferri

709 A, Cheng H, Ma J, Ren H, Chen QY, Yang Y, Qin S. FBXO32-mediated degradation of
710 PTEN promotes lung adenocarcinoma progression. Cell Death Dis. 2024 Apr
711 20;15(4):282.
712 26. Guo W, Zhang M, Shen S, Guo Y, Kuang G, Yang Z, Dong Z. Aberrant methylation
713 and decreased expression of the TGF-β/Smad target gene FBXO32 in esophageal
714 squamous cell carcinoma. Cancer, 2014, 120(16): 2412-2423.
715 27. Habel N, El-Hachem N, Soysouvanh F, Hadhiri-Bzioueche H, Giuliano S, Nguyen
716 S, Horák P, Gay AS, Debayle D, Nottet N, Béranger G, Paillerets BB, Bertolotto C,
717 Ballotti R. FBXO32 links ubiquitination to epigenetic reprograming of melanoma cells.
718 Cell death and differentiation, 2021, 28(6): 1837-1848.
719 28. Tang J, Wang S, Weng M, Guo Q, Ren L, He Y, Cui Z, Cong M, Qin M, Yu J, Su R,
720 Li X. The IGF2BP3-COPS7B Axis Facilitates mRNA Translation to Drive Colorectal
721 Cancer Progression. Cancer Res. 2023 Nov 1;83(21):3593-3610.
722 29. Chen LJ, Liu HY, Xiao ZY, Qiu T, Zhang D, Zhang LJ, Han FY, Chen GJ, Xu XM,
723 Zhu JH, Ding YQ, Wang SY, Ye YP, Jiao HL. IGF2BP3 promotes the progression of
724 colorectal cancer and mediates cetuximab resistance by stabilizing EGFR mRNA in an
725 m6A-dependent manner. Cell Death Dis. 2023 Sep 1;14(9):581.
726
727

728 **Figure Legends**

729 **Figure 1. Increased IGF2BP3 expression is associated with poor prognosis in GC**
730 **patients. (A-C)** Expression of 21 $m^6A$ related genes in the TCGA database, as well as
731 the GSE54129 and GSE66229 datasets. **(D)** Kaplan-Meier analysis of IGF2BP3
732 expression levels and overall survival in GC patients. **(E)** The expression levels of
733 IGF2BP3 mRNA in 50 pairs of GC and adjacent normal tissue samples were detected
734 by qRT-PCR. **(F)** Representative images showing IGF2BP3 protein expression levels
735 in 50 pairs of GC and adjacent normal tissue samples, as detected by IHC. Scale bar,
736 50 μm. Data are presented as means ± SD. $^{**}P < 0.01$, $^{***}P < 0.001$

737 **Figure 2. Knockdown of IGF2BP3 in GC cells suppresses cell proliferation,**
738 **migration and invasion *in vitro*. (A, B)** The expression of IGF2BP3 mRNA in HGC-
739 27 and MKN74 cells was detected by qRT-PCR. **(C, D)** The expression of IGF2BP3
740 protein in HGC-27 and MKN74 was detected by WB. **(E, F)** The effect of IGF2BP3
741 knockdown on the proliferation of HGC-27 and MKN74 cells was determined by the
742 CCK-8 assay. **(G, H)** The effect of IGF2BP3 knockdown on the migration of HGC-27
743 and MKN74 cells was assessed by the wound healing assay. Scale bar, 200 μm. **(I, J)**
744 The effect of IGF2BP3 knockdown on the migration of HGC-27 and MKN74 cells was
745 evaluated using the Transwell migration assay. Scale bar, 100 μm. **(K, L)** The effect of
746 IGF2BP3 knockdown on the invasion of HGC-27 and MKN74 cells was assessed using
747 Transwell invasion assay. Scale bar, 100 μm. **(M, N)** The effect of IGF2BP3 knockdown
748 on the apoptosis of HGC-27 and MKN74 cells was determined by flow cytometry. Data
749 are presented as means ± SD. $^{*}P < 0.05$, $^{**}P < 0.01$, $^{***}P < 0.001$, $^{****}P < 0.0001$

750 **Figure 3. Overexpression of IGF2BP3 in GC cells and human gastric mucosa cells**
751 **promotes cell proliferation, migration and invasion *in vitro*. (A, B)** The expression
752 of IGF2BP3 mRNA in MKN7 and GES-1 was detected by qRT-PCR. **(C, D)** The
753 expression of IGF2BP3 protein in MKN7 and GES-1 was detected by WB. **(E, F)** The
754 effect of IGF2BP3 overexpression on the proliferation of MKN7 and GES-1 cells was
755 assessed using the CCK-8 assay. **(G, H)** The effect of IGF2BP3 overexpression on the
756 migration of MKN7 and GES-1 cells was evaluated through a wound healing assay.
757 Scale bar, 200 μm. **(I, J)** The effect of IGF2BP3 overexpression on the migration of
758 MKN7 and GES-1 cells was determined utilizing a Transwell migration assay. Scale
759 bar, 100 μm. **(K)** The effect of IGF2BP3 overexpression on the invasion of MKN7 cells
760 was assessed via a Transwell invasion assay. Scale bar, 100 μm. **(L, M)** The effect of
761 IGF2BP3 overexpression on the apoptosis of MKN7 and GES-1 cells was analyzed by
762 flow cytometry. Data are presented as means ± SD. $^{**}P < 0.01$, $^{***}P < 0.001$, $^{****}P$
763 $< 0.0001$

764 **Figure 4. IGF2BP3 regulates the growth of GC *in vivo*. (A)** Nude mouse tumor-
765 bearing model. **(B)** Tumor growth curve. **(C, D)** Images (C) and weight (D) of
766 xenografted tumors were analyzed. **(E)** Representative images of tumor tissue sections
767 stained with HE. Scale bar, 50 μm. **(F)** Representative image of Ki67 IHC staining in
768 tumor tissue sections. Scale bar, 50 μm. Data are shown as means ± SD. $^{**}P < 0.01$,
769 $^{****}P < 0.0001$

770 **Figure 5. FBXO32 is the m$^6$A modification target of IGF2BP3. (A)** Differential
771 expression genes (DEGs) heat map identified by RNA-seq. **(B)** The number of DEGs

identified by RNA-seq. **(C)** The number of $m^6A$ peaks identified by MeRIP-seq. **(D)** $m^6A$ motif identified by MeRIP-seq. **(E)** The enrichment regions of $m^6A$ peaks on mRNA identified by MeRIP-seq. **(F)** The common genes between the siNC group and the siIGF2BP3 group in MeRIP-seq. **(G)** The enrichment regions of $m^6A$ peaks on mRNA identified by RIP-seq. **(H)** The number of $m^6A$ peaks identified by RIP-seq. **(I)** Genes identified by RIP-seq. **(J)** Overlap analysis of MeRIP-seq, RIP-seq and RNA-seq identified genes. **(K)** Expression of FBXO32 in GC paired tissue cohort from the TCGA database. **(L)** Subcellular localization of FBXO32 from GeneCards. **(M)** Kaplan-Meier analysis of FBXO32 expression levels and overall survival in patients with GC. **(N)** The $m^6A$ site and its abundance on FBXO32 transcripts were analyzed using IGV software. **(O)** The interaction between IGF2BP3 and FBXO32 was detected by RIP-qPCR. **(P)** Schematic diagram of the catRAPID website predicting the binding site between IGF2BP3 protein and FBXO32 mRNA.

**Figure 6. Expression of FBXO32 and its interaction with IGF2BP3 in GC. (A)** The expression of FBXO32 mRNA in GC cell lines and GES-1 was detected by qRT-PCR. **(B)** The expression of FBXO32 mRNA in 34 pairs of GC paired tissues was detected by qRT-PCR. **(C)** The basal expression of FBXO32 protein in cell lines was detected by WB. **(D)** The expression of FBXO32 protein in 19 pairs of GC paired tissues was detected by IHC. Scale bar, 50 μm. **(E)** Co-IP followed by WB analyses confirmed the binding between IGF2BP3 and FBXO32 in HGC-27 cells. **(F)** The distribution of IGF2BP3 and FBXO32 in HGC-27 cells was confirmed by Co-IF. Scale bar, 10 μm. **(G)** qRT-PCR was used to detect FBXO32 mRNA expression after IGF2BP3

knockdown in HGC-27 cells. **(H)** WB was used to detect FBXO32 protein expression after IGF2BP3 knockdown in HGC-27 cells. **(I)** qRT-PCR was used to detect FBXO32 mRNA expression after IGF2BP3 overexpression in MKN7 cells. **(J)** WB was used to detect FBXO32 protein expression after IGF2BP3 overexpression in MKN7 cells. Data are presented as means ± SD. *$P$ <0.05, **$P$ <0.01, ****$P$ <0.0001

**Figure 7. Oncogenic function of IGF2BP3 depends on FBXO32. (A)** The knockdown efficiency of four siRNA-FBXO32 sequences in MKN7 cells was assessed by qRT-PCR. **(B, C)** The expression of IGF2BP3 mRNA in HGC-27 (B) and MKN7 (C) cells was measured by qRT-PCR after co-transfection of respective siRNA and overexpression plasmid. **(D-H)** The effects of FBXO32 on IGF2BP3 in HGC-27 cells were detected by CCK-8 assay (D), colony formation assay (E), wound healing assay (F), Scale bar, 200 μm, Transwell migration assay (G) and Transwell invasion assay (H). Scale bar, 100 μm. **(I-M)** The effects of FBXO32 on IGF2BP3 in MKN7 cells were detected by CCK-8 assay (I), colony formation assay (J), wound healing assay (K), Scale bar, 200 μm, Transwell migration assay (L) and Transwell invasion assay (M). Scale bar, 100 μm. **(N)** Schematic illustration of the molecular mechanism of IGF2BP3 in GC. Data are presented as means ± SD. *$P$ <0.05, **$P$ <0.01, ***$P$ <0.001, ****$P$ <0.0001

## Supporting information

Additional supporting information may be found online in the Supporting Information section at the end of the article.

816 **Supplementary Figure**

817 **Supplementary Figure 1. IGF2BP3 affects glucose metabolism in GC cell lines. (A)**
818 The effect of IGF2BP3 expression level on glucose uptake in GC cells was determined
819 using a glucose uptake assay. **(B)** The effect of IGF2BP3 expression level on lactic acid
820 production in GC cells was determined by utilizing a lactic acid production assay. **(C)**
821 An ATP content assay showed the effect of IGF2BP3 expression level on ATP content
822 in GC cells.

823 **Supplementary Table**

824 Supplementary Table 1 The primer sequences of IGF2BP3, FBXO32, β-actin.

**Figure 1**

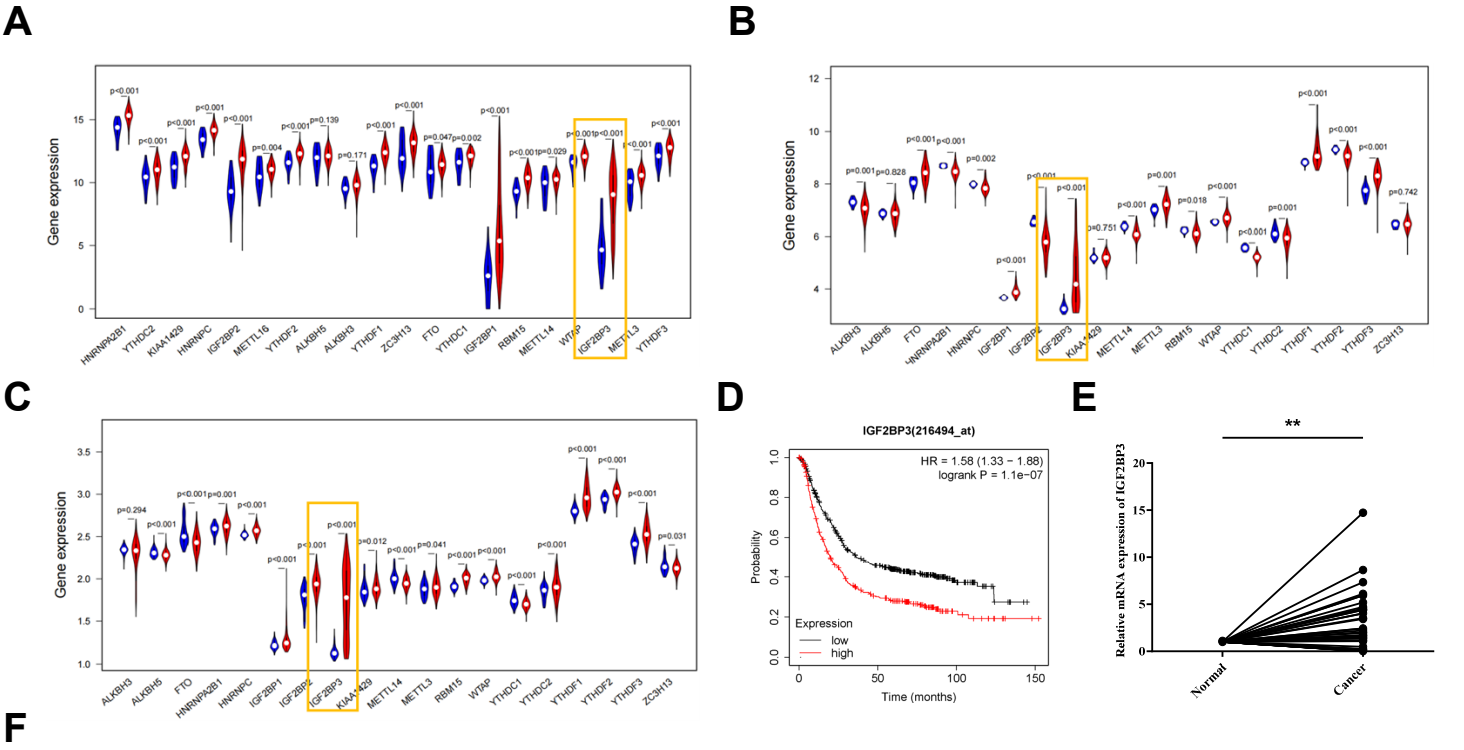


F

**Adjacent normal**

1 2 3

IGF2BP3

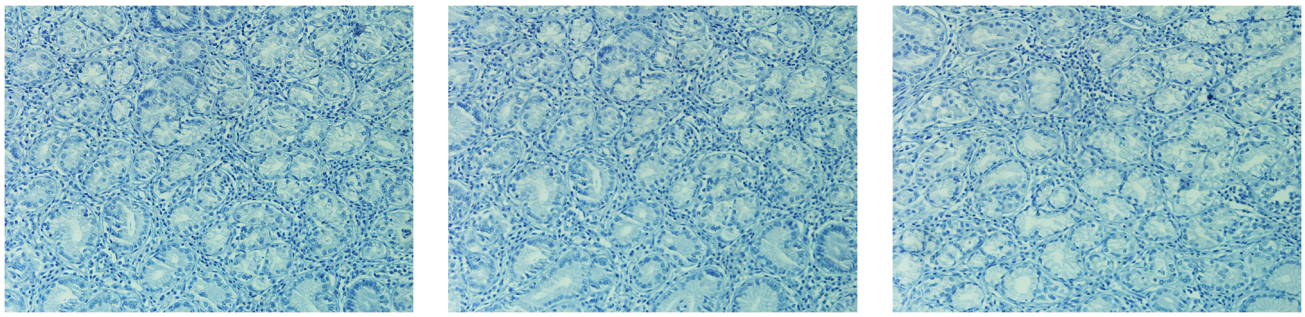

**Gastric cancer**

1 2 3

IGF2BP3

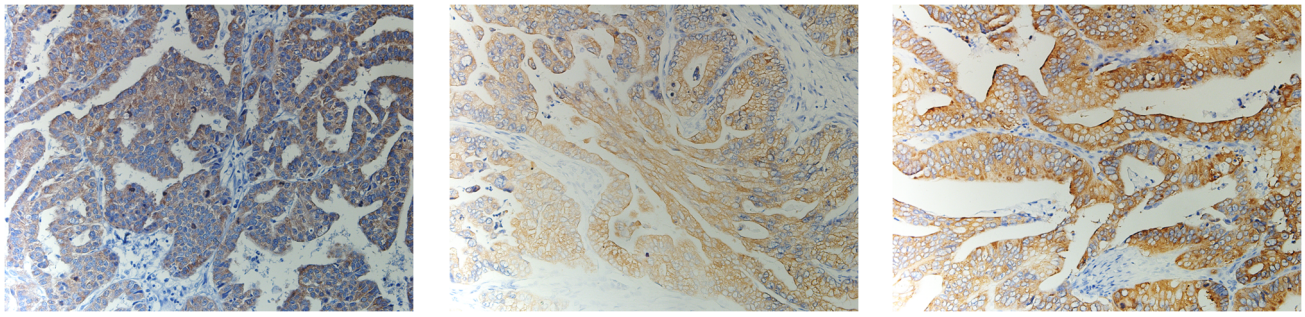

Figure 2

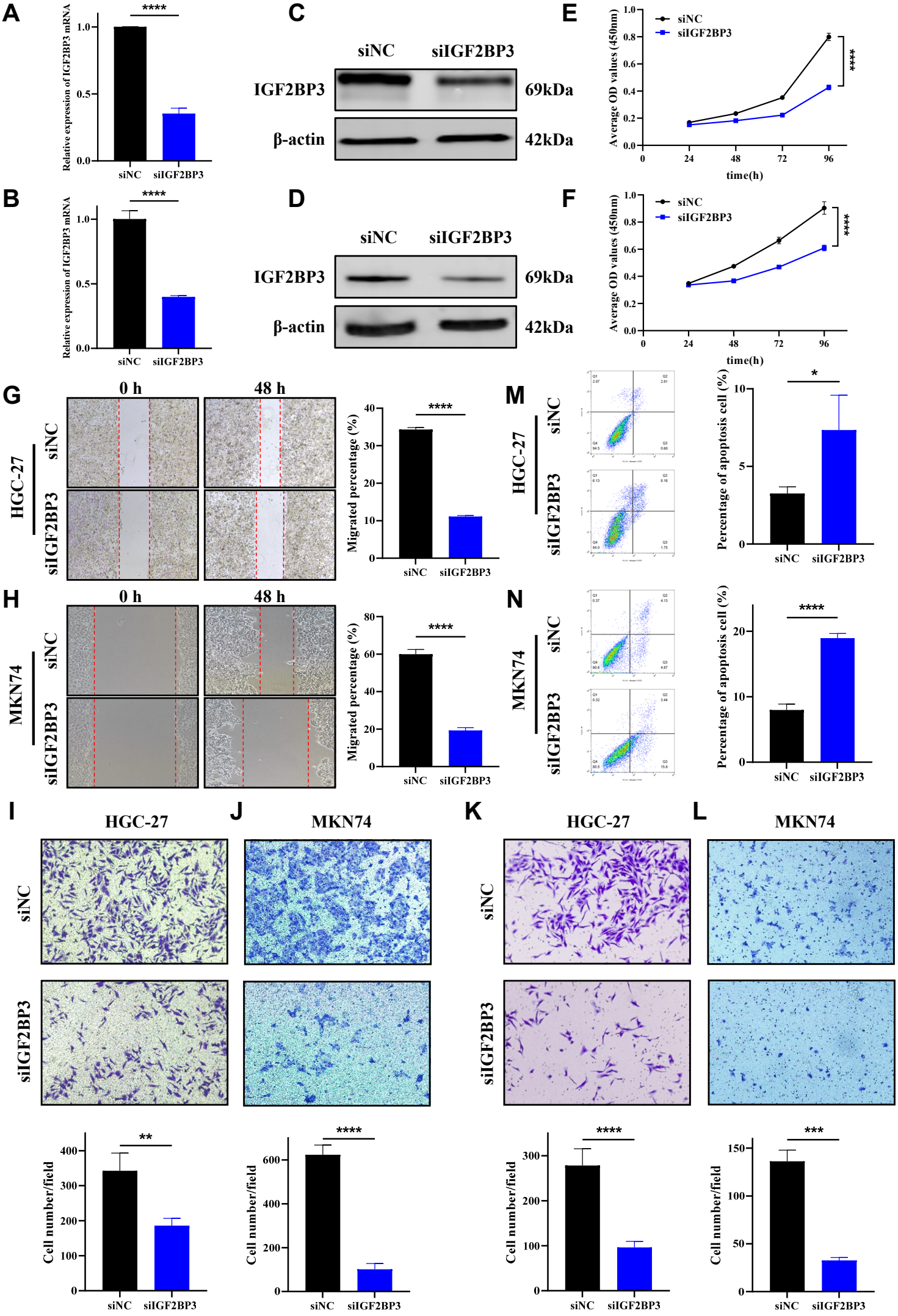
A
B
C
D
E
F
G
H
M
N
I
J
K
L
Relative expression of IGF2BP3 mRNA
siNC
siIGF2BP3
IGF2BP3
β-actin
69kDa
42kDa
Average OD values (450nm)
time(h)
0 h
48 h
HGC-27
MKN74
Migrated percentage (%)
Percentage of apoptosis cell (%)
Cell number/field

Figure 3

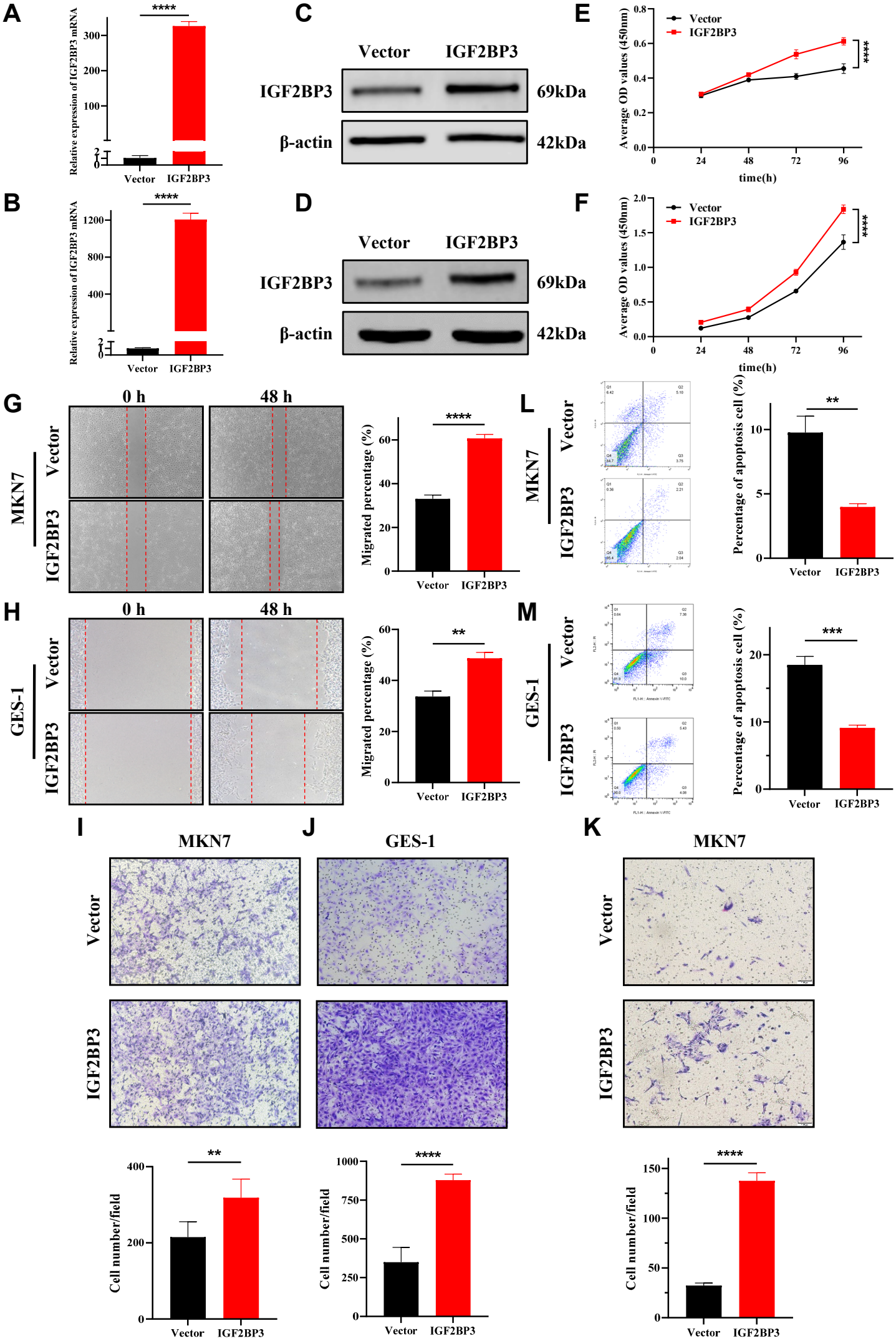
A
Relative expression of IGF2BP3 mRNA
****
Vector
IGF2BP3
B
Relative expression of IGF2BP3 mRNA
****
Vector
IGF2BP3
C
Vector
IGF2BP3
IGF2BP3
69kDa
β-actin
42kDa
D
Vector
IGF2BP3
IGF2BP3
69kDa
β-actin
42kDa
E
Average OD values (450nm)
Vector
IGF2BP3
****
time(h)
F
Average OD values (450nm)
Vector
IGF2BP3
****
time(h)
G
0 h
48 h
MKN7
Vector
IGF2BP3
Migrated percentage (%)
****
Vector
IGF2BP3
H
0 h
48 h
GES-1
Vector
IGF2BP3
Migrated percentage (%)
**
Vector
IGF2BP3
L
MKN7
Vector
IGF2BP3
Percentage of apoptosis cell (%)
**
Vector
IGF2BP3
M
GES-1
Vector
IGF2BP3
Percentage of apoptosis cell (%)
***
Vector
IGF2BP3
I
MKN7
Vector
IGF2BP3
Cell number/field
**
Vector
IGF2BP3
J
GES-1
Cell number/field
****
Vector
IGF2BP3
K
MKN7
Vector
IGF2BP3
Cell number/field
****
Vector
IGF2BP3

Figure 4

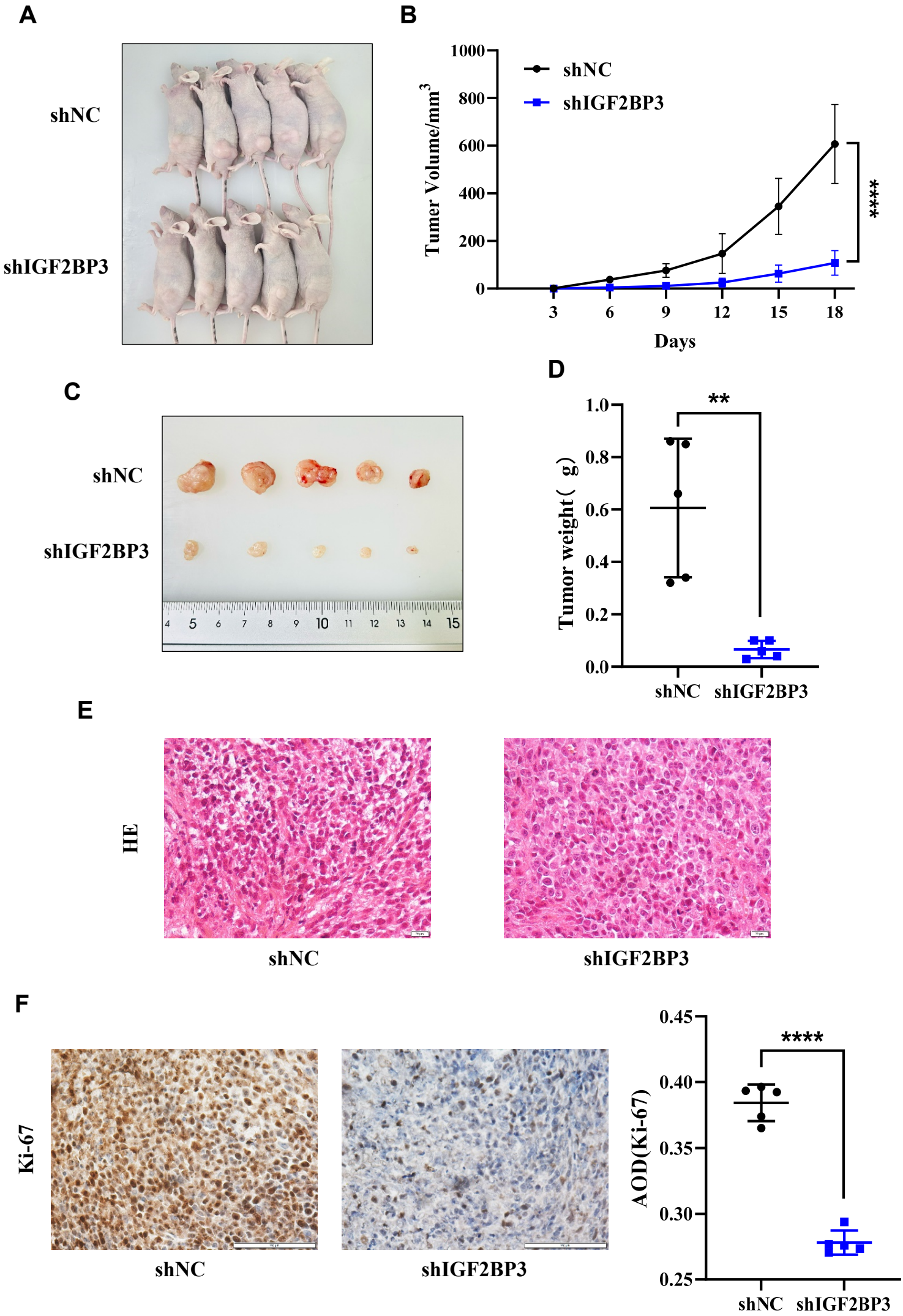
A
shNC
shIGF2BP3
B
shNC
shIGF2BP3
Tumer Volume/mm3
1000
800
600
400
200
0
3
6
9
12
15
18
Days
****
C
shNC
shIGF2BP3
D
Tumor weight( g)
1.0
0.8
0.6
0.4
0.2
0.0
**
shNC
shIGF2BP3
E
HE
shNC
shIGF2BP3
F
Ki-67
shNC
shIGF2BP3
AOD(Ki-67)
0.45
0.40
0.35
0.30
0.25
****
shNC
shIGF2BP3

Figure 5

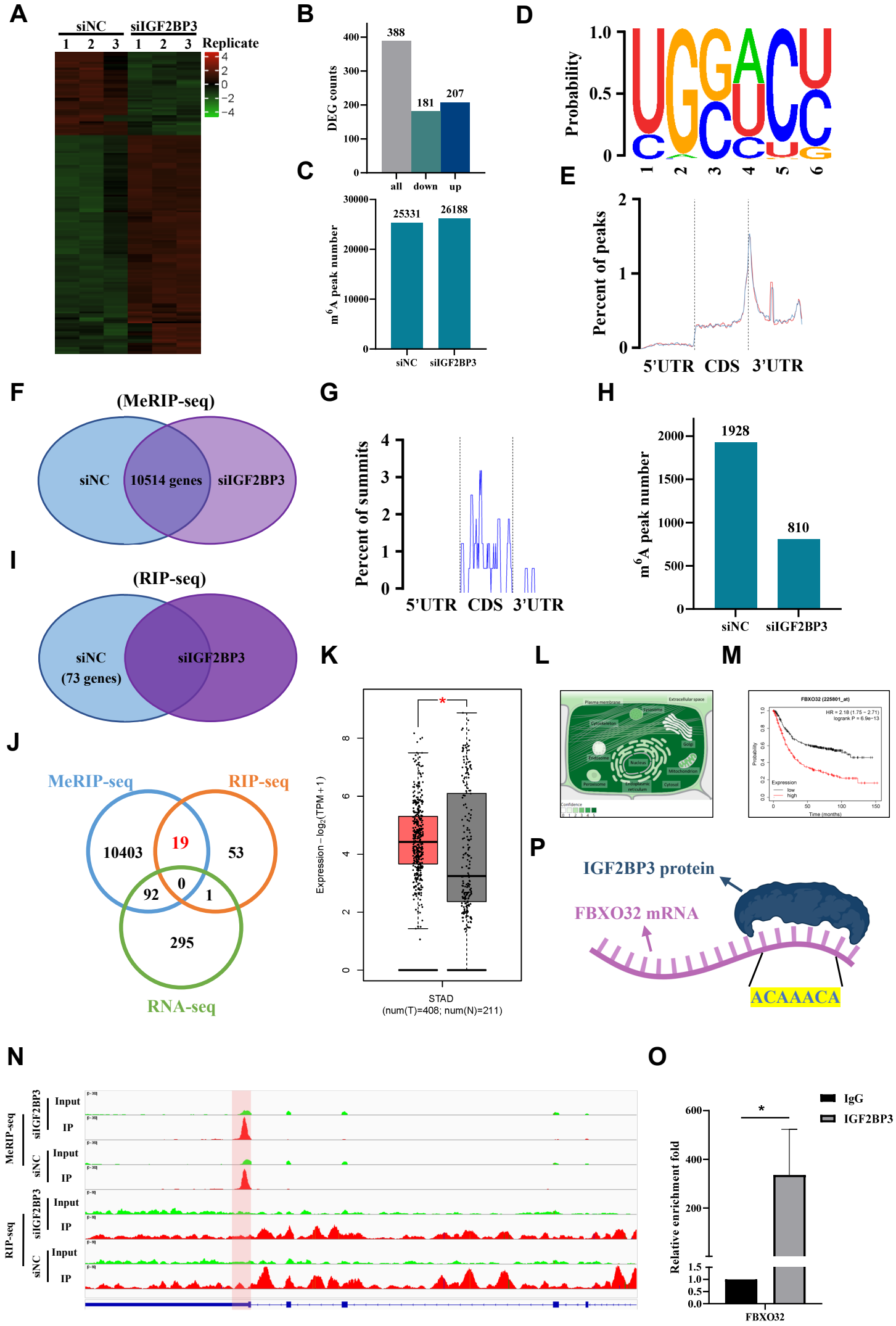
A
siNC
siIGF2BP3
1 2 3 1 2 3
Replicate
4
2
0
−2
−4
B
DEG counts
388
181
207
all
down
up
C
m6A peak number
25331
26188
siNC
siIGF2BP3
D
Probability
1.0
0.5
0
1 2 3 4 5 6
E
Percent of peaks
5'UTR CDS 3'UTR
F
(MeRIP-seq)
siNC
10514 genes
siIGF2BP3
G
Percent of summits
5'UTR CDS 3'UTR
H
m6A peak number
1928
810
siNC
siIGF2BP3
I
(RIP-seq)
siNC
(73 genes)
siIGF2BP3
J
MeRIP-seq
RIP-seq
RNA-seq
10403
19
53
0
92
1
295
K
Expression – log2(TPM+1)
STAD
(num(T)=408; num(N)=211)
L
M
FBXO32 (225801_at)
HR = 2.18 (1.75 – 2.71)
logrank P = 6.9e−13
Expression
low
high
Time (months)
P
IGF2BP3 protein
FBXO32 mRNA
ACAAACA
N
MeRIP-seq
siIGF2BP3
siNC
RIP-seq
Input
IP
O
IgG
IGF2BP3
Relative enrichment fold
FBXO32

Figure 6

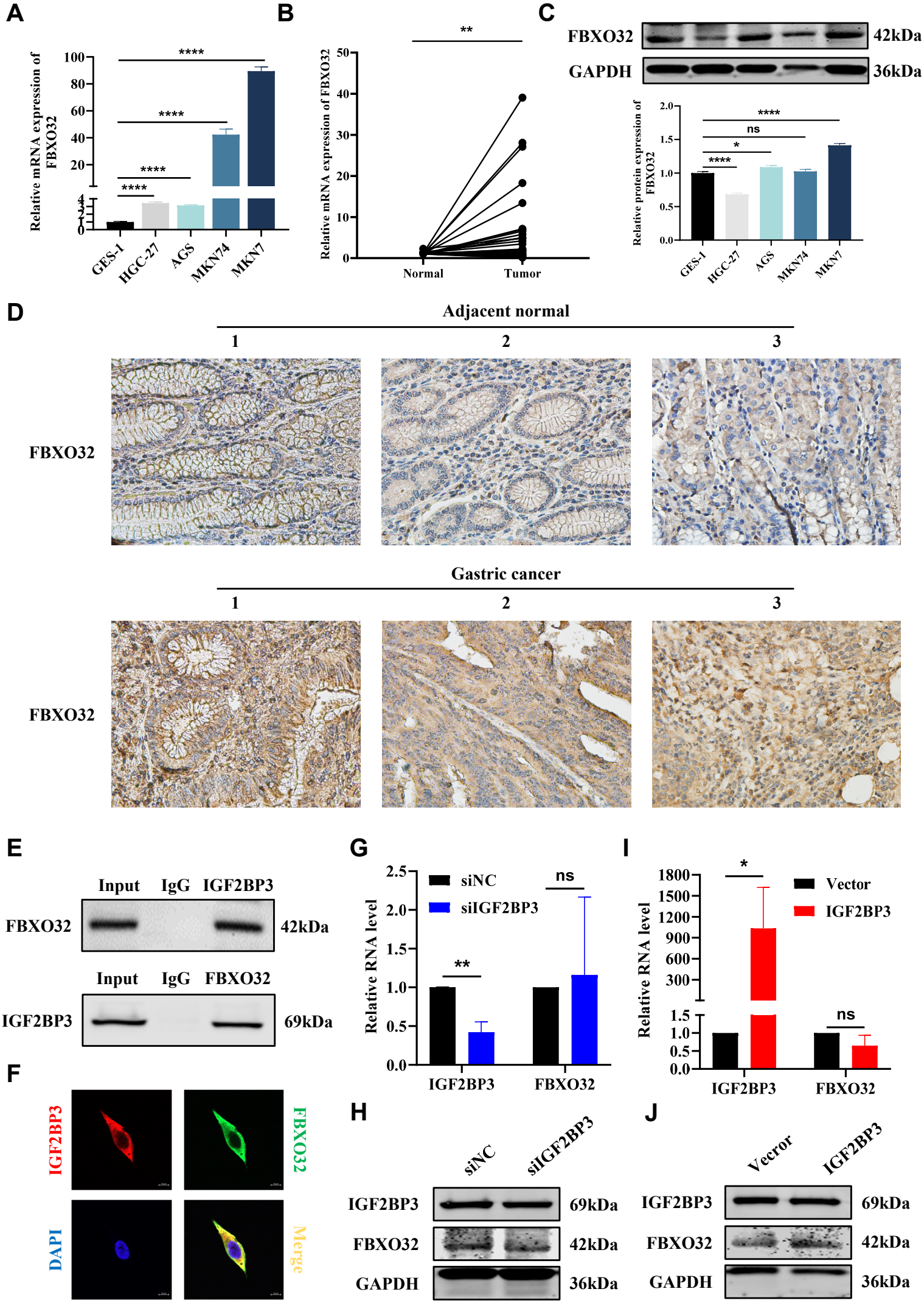
A
Relative mRNA expression of FBXO32
100
80
60
40
20
4
3
2
1
0
****
****
****
****
GES-1
HGC-27
AGS
MKN74
MKN7
B
Relative mRNA expression of FBXO32
50
40
30
20
10
0
**
Normal
Tumor
C
FBXO32
42kDa
GAPDH
36kDa
Relative protein expression of FBXO32
2.0
1.5
1.0
0.5
0.0
****
ns
*
****
GES-1
HGC-27
AGS
MKN74
MKN7
D
Adjacent normal
1
2
3
FBXO32
Gastric cancer
1
2
3
FBXO32
E
Input
IgG
IGF2BP3
FBXO32
42kDa
Input
IgG
FBXO32
IGF2BP3
69kDa
F
IGF2BP3
FBXO32
DAPI
Merge
G
Relative RNA level
2.5
2.0
1.5
1.0
0.5
0.0
siNC
siIGF2BP3
**
ns
IGF2BP3
FBXO32
I
Relative RNA level
1800
1500
1200
900
600
300
1.5
1.0
0.5
0.0
*
ns
Vector
IGF2BP3
IGF2BP3
FBXO32
H
siNC
siIGF2BP3
IGF2BP3
69kDa
FBXO32
42kDa
GAPDH
36kDa
J
Vecror
IGF2BP3
IGF2BP3
69kDa
FBXO32
42kDa
GAPDH
36kDa

Figure 7

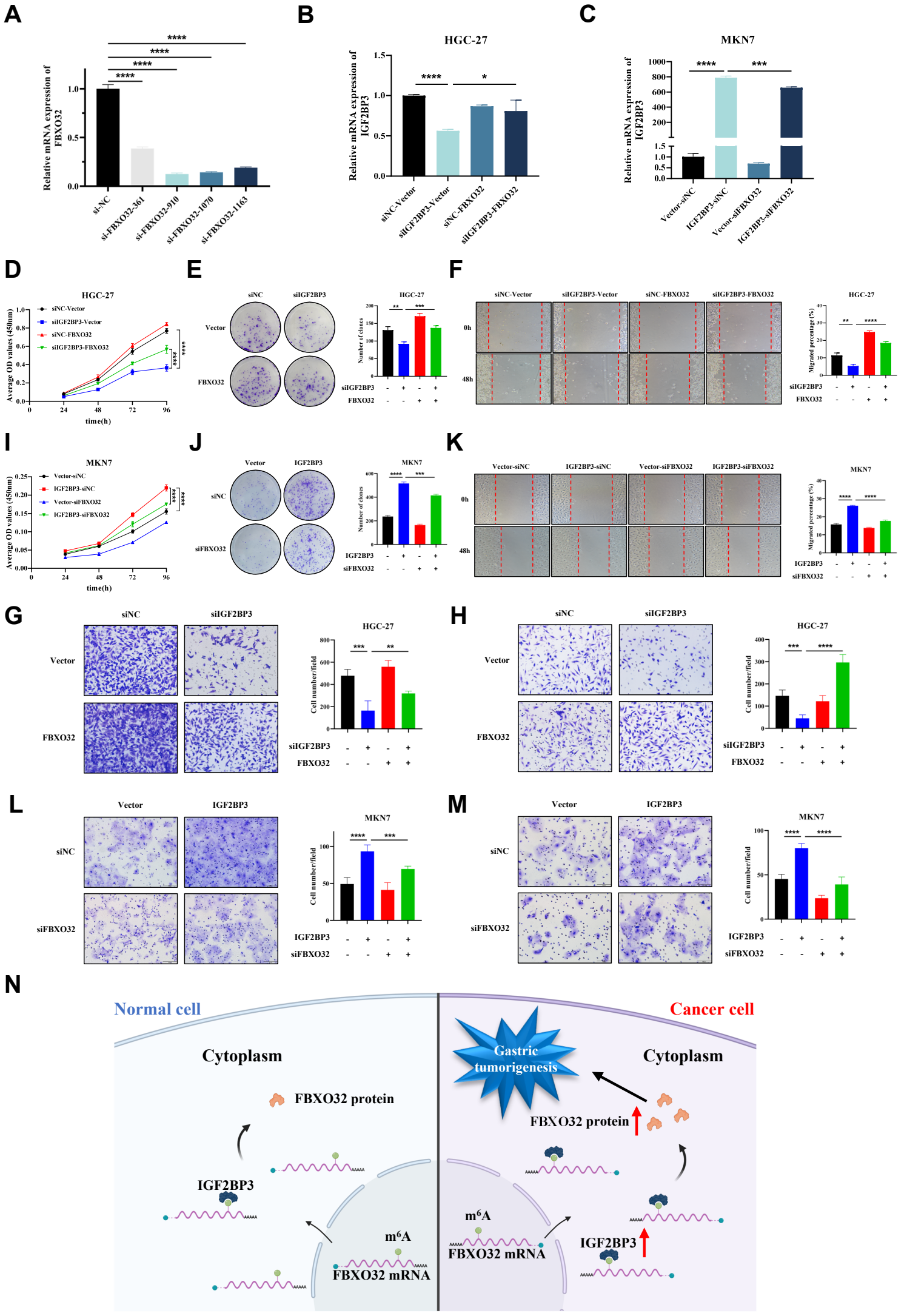
A
Relative mRNA expression of FBXO32
si-NC
si-FBXO32-361
si-FBXO32-910
si-FBXO32-1070
si-FBXO32-1163
B
HGC-27
Relative mRNA expression of IGF2BP3
siNC-Vector
siIGF2BP3-Vector
siNC-FBXO32
siIGF2BP3-FBXO32
C
MKN7
Relative mRNA expression of IGF2BP3
Vector-siNC
IGF2BP3-siNC
Vector-siFBXO32
IGF2BP3-siFBXO32
D
HGC-27
Average OD values (450nm)
time(h)
E
siNC
siIGF2BP3
Vector
FBXO32
Number of clones
F
siNC-Vector
siIGF2BP3-Vector
siNC-FBXO32
siIGF2BP3-FBXO32
0h
48h
Migrated percentage (%)
I
MKN7
Vector-siNC
IGF2BP3-siNC
Vector-siFBXO32
IGF2BP3-siFBXO32
J
Vector
IGF2BP3
siNC
siFBXO32
K
G
H
L
M
Cell number/field
N
Normal cell
Cancer cell
Cytoplasm
FBXO32 protein
IGF2BP3
m6A
FBXO32 mRNA
Gastric tumorigenesis

**Table 1 The expression level of IGF2BP3 protein in two groups**

| Group | Cases | IGF2BP3 expression | | Positive Rate(%) | $\chi^2$ | *P* |
|---|---|---|---|---|---|---|
| | | Postive | Negative | | | |
| Gastric cancer tissues | 50 | 26 | 24 | 52% | 18.382 | 0.0001*** |
| Adjacent normal tissues | 50 | 6 | 44 | 12% | | |

**Table 2 The relationship between the expression of IGF2BP3 in gastric cancer tissue and the clinicoapathological data of patients**

| Group | Cases | IGF2BP3 expression | | $\chi^2$ | *P* |
|---|---|---|---|---|---|
| | | Postive | Negative | | |
| Gender | | | | | |
| Male | 39 | 23 | 16 | 3.455 | 0.063 |
| Female | 11 | 3 | 8 | | |
| Age (years) | | | | | |
| ≦60 | 22 | 11 | 11 | 0.063 | 0.802 |
| > 60 | 28 | 15 | 13 | | |
| Tumor size (cm) | | | | | |
| ≦4 cm | 23 | 13 | 10 | 0.349 | 0.555 |
| > 4 cm | 27 | 13 | 14 | | |
| Differentiation | | | | | |
| Poorly | 28 | 17 | 11 | 1.936 | 0.164 |
| Well | 22 | 9 | 13 | | |
| Lymphnode metastasis | | | | | |
| Absent | 17 | 4 | 13 | 8.365 | 0.004** |
| Present | 33 | 22 | 11 | | |
| TNM Staging | | | | | |
| I + II | 21 | 5 | 16 | 11.528 | 0.001** |
| III + IV | 29 | 21 | 8 | | |